ChemElectroChem

Chemistry Europe
European Chemical Societies Publishing
ChemElectroChem

RESEARCH ARTICLE OPEN ACCESS

Exploring Mediated Electron Transfer in *Vibrio natriegens*

Daniel Barón Díaz[1] | Caty Kai-Ting Wang[1] | Deria Kabova[2] | Stefan Frielingsdorf[2] | Dirk Holtmann[1]

[1]Institute of Process Engineering in Life Sciences 2 - Electrobiotechnology, Karlsruhe Institute of Technology, Karlsruhe, Germany | [2]Department of Chemistry, Technische Universität Berlin, Berlin, Germany

Correspondence: Dirk Holtmann (dirk.holtmann@kit.edu)

Received: 6 July 2026 | **Revised:** 1 September 2026 | **Accepted:** 2 September 2026

Keywords: bioelectrochemical systems | redox mediators | *Vibrio natriegens*

ABSTRACT

Vibrio natriegens is a promising biotechnological chassis distinguished by exceptionally rapid growth and dynamic metabolism. This microorganism can deliver electrons both directly to electrodes via the well-established MtrCAB electron export system, as well as mediated through redox shuttle molecules. Notably, mediated electron transfer (MET) results in higher currents. Bioelectrochemical systems offer a possibility to influence the metabolic product spectrum of *V. natriegens* by using a poised anode as terminal electron acceptor. This study systematically evaluated twelve mediators spanning a redox potential window from −520 to +490 mV versus Ag/AgCl (3 M KCl) to establish efficient MET in *V. natriegens*. Among the tested compounds, potassium ferricyanide yielded the highest current densities ($104 \pm 20\,\mu A\,cm^{-2}$) and faradaic efficiency. Interestingly, riboflavin underwent less than 0.05 cycles of shuttling, indicating a low electron shuttling capability. In contrast, phenazines demonstrated efficiency for electron uptake from *V. natriegens* cells, but the current production was unstable. Overall, a specific redox potential window above −220 mV versus Ag/AgCl was identified within which mediator reduction occurred most efficiently. These findings establish a catalog of compatible redox shuttles and lay the basis for increased efficiency of bioelectrochemical processes leveraging *V. natriegens*.

1 | Introduction

Vibrio natriegens is a promising chassis for biotechnology, distinguished by its exceptionally high growth rate and dynamic metabolism, which could significantly increase bioprocess efficiencies. This nonpathogenic bacterium can utilize over 60 different carbon sources and has an extensive genetic toolkit available [1, 2]. Under ideal conditions, *V. natriegens* has a doubling time of under ten minutes and a glucose uptake rate about twice as fast as *E. coli* [3, 4]. Under anaerobic conditions, *V. natriegens* ferments glucose to a variety of organic acids and partially oxidized metabolites [2]. Additionally, it can export electrons outside the cell via the canonical MtrCAB pathway [5]. The combination of these two strategies to get rid of excess electrons offers the possibility of conduct anodic electrofermentation. Using the electrode as terminal electron acceptor, the product spectrum can be influenced to enhance the yield in an anaerobic process [6].

Although *V. natriegens* is electroactive [5], its propensity for poor biofilm formation restricts its efficiency to transfer electrons directly to an anode [7]. Mediated BES, which employ added redox molecules to shuttle electrons between bacteria and an electrode, present a robust alternative [8]. Compared to direct electron transfer, mediated electron transfer (MET) increases the interaction surface as dissolved mediators are present in the complete reactor volume and microbial electron transfer is not limited to biofilm-dependent physical contact with the electrode. Through this principle, the use of redox mediators can increase electron-transfer rates by orders of magnitude, even when naturally electroactive bacteria are used [7, 9].

While previous studies have demonstrated the ability of *V. natriegens* to reduce specific mediators such as ferricyanide, methylene blue, and phenazines [7, 10], no comprehensive screening has yet been conducted to compare these and other promising redox mediators demonstrated for *V. natriegens* and other gram-negative bacteria. There is a need to identify an optimal mediator that balances biocompatibility, aqueous solubility, and affinity for bacterial interaction sites. To address this gap, we present a comprehensive screening of a catalog of twelve redox mediators spanning a potential window from −520 to +490 mV versus Ag/AgCl (3 M KCl) in a miniaturized BES allowing simultaneous electrochemical and spectrophotometric analysis [11]. This study aims to identify the most effective candidate for shuttling electrons from *V. natriegens* to a poised anode, thereby establishing a foundation for electrochemically controlled bioprocesses.

2 | Results and Discussion

2.1 | Maximal Mediator Reduction Rates

Experiments using glucose as carbon and energy source were conducted to evaluate twelve redox mediators commonly used for MET, spanning a redox potential window of approximately 1 V. From the photometric measurements for each tested mediator, kinetic data on microbial mediator reduction can be derived. By correlating the drop in absorbance over time with concentration via established calibration curves at the characteristic wavelength for each mediator [12], the maximal reduction rates were determined (Table 1). The maximal reduction rate was most commonly reached at the beginning of the experiment, shortly after inoculation. Among the tested compounds, FEC exhibited the highest reduction rate. However, FEC was utilized at the highest concentration among all mediators due to its high solubility in aqueous media. Since mediator reduction frequently follows first-order kinetics [13], in which the reaction rate is directly proportional to the substrate concentration, the substantially higher reduction rate of FEC reflects its higher availability to the cells rather than an inherently superior turnover rate. Consistent with the high reduction rate, FEC also generated the highest measured current densities.

Interestingly, high initial reduction rates did not always equal high current densities. For example, 2,6-Dichlorophenolindophenol (DCIP) was reduced very quickly ($131.21 \pm 24.63\,\mu mol\,L^{-1}h^{-1}$) by the cells at the beginning of the experiment (Figure S1). However, despite the fast reduction kinetics, the system failed to sustain a stable maximal current density over time, reaching $9.49 \pm 3.94\,\mu A/cm^2$, demonstrating a decoupling between the initial biological reduction rate and sustained electron flux to the electrode. Additionally, glucose remained largely unconsumed (>80%) in this experiment. Both of these observations suggest that DCIP had an inhibitory effect on *V. natriegens*' metabolism. Similarly, PMS demonstrated rapid initial reduction kinetics and high currents relative to the mediator concentration in the medium. However, the current output dropped after the first 2 h, limiting long-term power generation despite favorable initial kinetics.

Interestingly, riboflavin (RF) yielded very low current densities around $0.5\,\mu A\,cm^{-2}$ throughout the experiment, and no significant reduction could be detected photometrically. This suggests that under the applied cultivation conditions, the redox potential of

TABLE 1 | Maximal reduction rates determined by absorbance change at the specific characteristic wavelength for the oxidized/reduced species. The reduction rate was calculated using calibration lines containing different mediator concentrations in the relevant range. Due to missing absorbance drops at the corresponding characteristic wavelengths, DHB, RF, and NR reduction could not be detected by photometric measurements. 2,2′-azino-bis (3-ethylbenzothiazoline-6-sulfonic acid) (ABTS), potassium ferricyanide (FEC), methylene blue (MB), neutral red (NR), resorufin (RES), phenazine carboxylic acid (PCA) and riboflavin (RF) ($n = 3$); methyl red (MR), 2,6-dichlorophenolindophenol (DCIP), phenazine ethosulfate (PES) and phenazine methosulfate (PMS) ($n = 4$); 2,3-dihydroxybenzoic acid (DHB) ($n = 5$). The redox potentials were determined using CV scans at 10 mV s^{-1} (Figure S2) in M1 minimal medium, whereas the E_m for MR was taken from literature, as CV scans would degrade the mediator in this system [11].

Mediator	Redox potential, mV versus Ag/AgCl (3 M KCl)	Concentration, μmol L^{-1}	Maximal reduction rate, μmol L^{-1} h^{-1}	Maximal current density, μA cm^{-2}
ABTS	490	100	80.60 ± 5.11	9.22 ± 1.56
FEC	210	1000	571.25 ± 15.00	104.32 ± 19.48
MR	206	50	61.78 ± 0.87	13.22 ± 1.86
DHB	185	120	—	16.54 ± 8.00
DCIP	48	80	131.21 ± 24.63	9.49 ± 3.94
PMS	−100	50	103.84 ± 5.91	10.04 ± 1.85
PES	−133	50	49.31 ± 14.75	12.45 ± 5.38
PCA	−220	5	35.00 ± 12.70	0.51 ± 0.37
RES	−248	100	8.93 ± 0.24	5.38 ± 3.82
MB	−250	20	49.20 ± 1.68	2.86 ± 0.63
RF	−405	100	—	0.49 ± 0.23
NR	−520	100	—	—

RF is unfavorable for efficient reduction by *V. natriegens*. This is consistent with previous experiments conducted by Gong and coworkers, in which RF only marginally increased current generation in a BES cultivation using complex medium [10]. However, to confirm that the gold surface of the electrode is not negatively affecting the interaction with RF, we conducted additional experiments comparing MET using carbon- and gold screen-printed electrodes in triplicate. We found no significant difference in cell growth, mediator shuttling, or glucose consumption between the two materials (Figure S4). It is remarkable that RF reduction in *V. natriegens* behaves differently from *Shewanella oneidensis* MR-1, which uses RF naturally as a highly effective electron shuttle for its MtrCAB [14]. Even though the MtrCAB systems of *V. natriegens* ATCC 14048 and *S. oneidensis* MR-1 have significant sequence similarity (33% for MtrC, 63% for MtrA, and 47% for MtrB) [5], it is plausible that the *V. natriegens* complex interacts with redox shuttles through distinct mechanistic pathways or steric constraints.

2.2 | Average Cycles Undergone per Redox Molecule

To be able to compare reduction rates in experiments with variable redox shuttle concentrations, the average cycle per molecule was calculated according to Gemünde and coworkers [11]. The total cycles per molecule observed represent a complex interplay of factors, including mediator solubility, accessibility to cellular interaction sites, cytotoxicity, and chemical stability in the medium [11]. The 10 h timeframe was selected as it marked the point at which the integrated current for the experiments began to stagnate, allowing to have a fair basis for comparison between the different mediators. Among the twelve candidates tested, FEC and MR exhibited the highest number of redox cycles per molecule over a 10 h period (Figure 1). This indicates a high affinity of *V. natriegens* for reducing these compounds as the interaction is normalized by the available concentration in the bulk.

A comparative analysis with a similar redox screening conducted for *Cupriavidus necator* [12] helps to further contextualize the findings in *V. natriegens*. It is notable that *C. necator* achieved reduction of several redox mediators such as FEC, MR, DCIP, MB, PMS, and PES despite lacking native EET mechanisms, demonstrating that mediator interaction is not strictly dependent on dedicated EET machinery like MtrCAB but also takes place due to unspecific diffusion to the periplasmic space or even the cytoplasm of the microbial cell. The maximal reduction rate for FEC in *V. natriegens* was approximately 10 times faster than that observed in *C. necator* [12], aligning well with the difference in EET capabilities. In contrast, *C. necator*, which lacks native EET mechanisms, reduced PMS at a maximal rate approximately 20 times faster than *V. natriegens*. The unexpected divergence in phenazine reduction kinetics may be explained by the differences in experimental cultivation conditions and the fact that the reduction rates are not normalized to the cultivated biomass. In our experiments, the reduction of PMS reached its limit with the end of growth. In contrast, *C. necator* was cultivated under conditions that supported active proliferation. Therefore, the superior phenazine reduction rates in *C. necator* compared to the growth-arrested *V. natriegens* suggest that phenazine-MET may be more strongly coupled to biomass growth than FEC-mediated transfer or that the lack of nitrogen availability in *V. natriegens* specifically limits the turnover of phenazine-based shuttles.

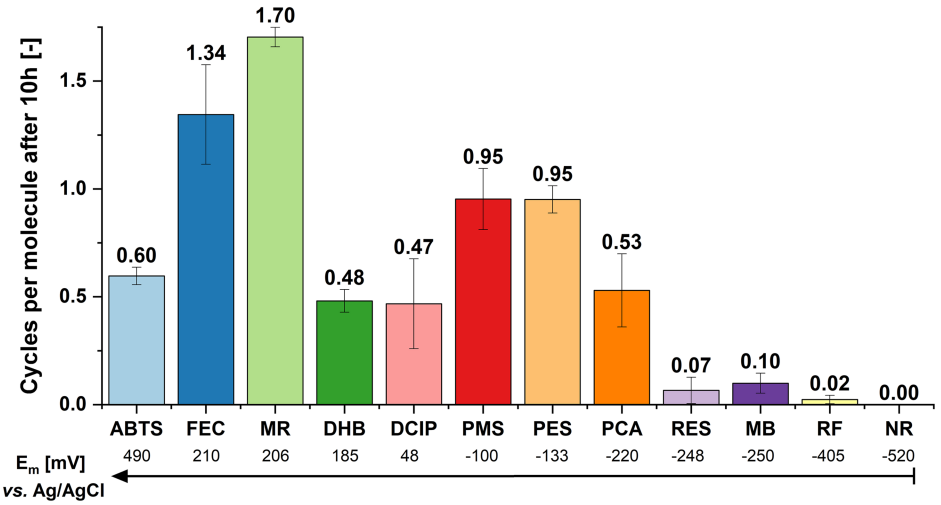

FIGURE 1 | *Vibrio natriegens* is more efficient at reducing redox mediators with a redox potential higher than −220 mV versus Ag/AgCl (3 M KCl) using glucose as a carbon and energy source. The average cycles per molecule after 10 h for the investigated redox mediators plotted against their redox potential E_m versus Ag/AgCl is shown. The redox potentials of the mediators were determined in the miniaturized BES using CV scans at 10 mV s^{-1} (Figure S2), whereas the E_m for MR was taken from literature, as CV scans would degrade the mediator in this system [5]. The average cycles per molecule are calculated by integrating the current time curves over the first 10 h after inoculation and dividing that charge with the amount of charge a single molecule of mediator can transport per reduction/oxidation cycle. The integration until 10 h after inoculation was chosen as it is the time point at which the current production in the first experimental setup stagnated (data not shown). 2,2′-azino-bis (3-ethylbenzothiazoline-6-sulfonic acid) (ABTS), potassium ferricyanide (FEC), methylene blue (MB), neutral red (NR), resorufin (RES), phenazine carboxylic acid (PCA) and riboflavin (RF) ($n = 3$); methyl red (MR), 2,6-dichlorophenolindophenol (DCIP), phenazine ethosulfate (PES) and phenazine methosulfate (PMS) ($n = 4$); 2,3-dihydroxybenzoic acid (DHB) ($n = 5$). Numbers above bars indicate the mean of n biological replicates. The error bars indicate the standard deviation of the replicates. Arrowed line indicates the direction of increasing redox potential.

The observed reduction of ABTS through *V. natriegens* cells, contrasted with the complete lack of activity in *C. necator*, highlights a fundamental mechanistic difference between the two organisms, likely driven by mediator permeability and surface accessibility. ABTS might exclusively act through extracellular interaction sites because it is a highly charged, hydrophilic diammonium salt unlikely to penetrate the hydrophobic lipid bilayer of gram-negative bacteria [12, 15]. This membrane exclusion is supported by the screening data in *C. necator*, where ABTS yielded a total turnover number of zero over 118 h despite demonstrating the least impact on cell growth among tested mediators, indicating that the molecule remains external and cannot access the internal interaction sites [12, 16]. Unlike the smaller FEC molecule, which could traverse the gram-negative outer membrane via unspecific porins [12, 15] or TonB-dependent active transport [17] to undergo reduction within the periplasm, the steric and electrostatic properties of ABTS make such nonspecific translocation highly unlikely [12, 15]. Consequently, the ability of *V. natriegens* to reduce ABTS suggests that this interaction occurs exclusively at the cell exterior. This mechanism aligns with findings in *S. oneidensis*, in which the decaheme cytochrome MtrC, located on the extracellular face of the outer membrane [18], has been shown to directly interact with ABTS in solution [19]. Therefore, ABTS could be a suitable alternative to commonly used metal oxides for probing EET, thereby making photometric assays easier to carry out by eliminating problems related to the possible interference or sedimentation of insoluble material.

From all the tested mediators, we identified a specific redox potential window from −220 mV up to 490 mV versus Ag/AgCl (3 M KCl), within which mediator reduction was significantly more active. This suggests a redox potential window for efficient MET. When compared to the redox potential of the MtrCAB homolog in *S. oneidensis*, which possesses a redox potential window from fully oxidized at −197 mV to fully reduced at −647 mV versus Ag/AgCl (sat. KCl) [20], the observation that reduction activity is more active in general using redox mediators above −220 mV versus Ag/AgCl (3 M KCl), independently of the molecule's hydrophilicity, aligns well with the explanation of a stronger interaction of these mediators with *V. natriegens* MtrCAB hemes in the bulk. The fact that RES and MB showed significantly less shuttling activity than PCA despite having a similar redox potential suggests a cut-off potential up to which efficient electron transfer is possible from *V. natriegens* MtrCAB system. Consistent with previous studies highlighting the role of phenazines for MET in *V. natriegens*, phenazine compounds demonstrated considerable activity in this screening [10].

2.3 | Glucose Consumption and Faradaic Efficiency

Even though the average cycles per molecule are useful to compare the efficiency of electron shuttling across different concentrations, the main goal for a BES should be to maximize the overall obtained current densities and the faradaic efficiencies, independent of the mediator concentration. Therefore, at the end of the experiment, the total electron output remains the decisive metric for performance. Normalization enables meaningful comparisons between mediators with vastly different solubilities and toxicities and allows poorly soluble or highly toxic compounds to be evaluated alongside more soluble and biocompatible alternatives. However, in mediated systems, one of two cases limits current densities: (i) anode regeneration or (ii) microbial reduction of the mediator. In the first case, increasing mediator concentrations would facilitate mass transfer to the anode and should therefore increase current output until inhibition negatively affects microbial activity. In the second case, decreasing the concentration should not negatively affect current output as oxidized mediator is available in excess. In the latter case, the current density would largely remain constrained by the biological activity, and higher concentrations would result in decreased cycles per molecule while maintaining comparable current densities. Therefore, besides evaluating the cycles per molecule metric, analyzing glucose consumption and faradaic efficiency is essential.

Therefore, to further evaluate the suitability of the screened mediators to generate current, glucose consumption was analyzed via HPLC for each mediator at the end of the experiment (Figure 2). Out of this data, the faradaic efficiency (FE) was determined after subtracting the charge routed into organic acids and ethanol. FE was the highest with FEC, a result attributed to the overall efficiency of electron transfer facilitated by the higher concentration of this redox mediator in the BES. In general, the FE is low when compared to other electroactive bacteria that depend only on EET. This can be explained by the ability of *V. natriegens* to dispose of electrons via fermentative pathways [2]. Additionally, the FEC experiment was ended before current decline, therefore making the theoretical FE higher if the experiment had been carried out for longer. Nonetheless, an FE of 2.3% was reached in a stirred tank bioreactor setup with FEC as a redox mediator [5], therefore making the calculated FE of 5% ± 2.1% in this study lie within the expected range. Even though methyl red (MR) outperforms all other mediators in the cycles per molecule metric (Figure 1), its limited aqueous solubility combined with its lower FE makes it less suitable for practical applications than FEC. Due to measurement uncertainties, the electron balancing using the produced organic acids for PMS and PES resulted in values over 100%, making the calculation of FE, considering the organic acids, not feasible. Therefore, for those two mediators, the percentage of electrons transferred from the consumed glucose to the anode is reported in Figure 2. For better comparison, the same metric is provided for all redox mediators in the Supporting Information (Figure S5).

Analysis of glucose consumption revealed that only DCIP and RES caused significant reduction in glucose uptake during cultivation, suggesting inhibitory effects at the concentrations used, while all other cultures consumed glucose to similar extents (Figure 2). These findings align with literature reporting strong DCIP inhibition in *C. necator* even below 1 mM (IC_{50} = 0.05 mM), though *V. natriegens* appears relatively more sensitive to RES than *C. necator* [16]. For all other mediators, the similar extent of glucose consumption demonstrates that differences in mediator reduction efficiency (Figure 1) were not caused by inherent metabolic inhibition but rather reflect limitations in the electron-transfer pathway to the anode itself. Although lowering DCIP and RES concentrations might alleviate cellular stress, it would likely compromise anodic mediator regeneration and overall BES efficiency. Mediators requiring low μM or nM concentrations for

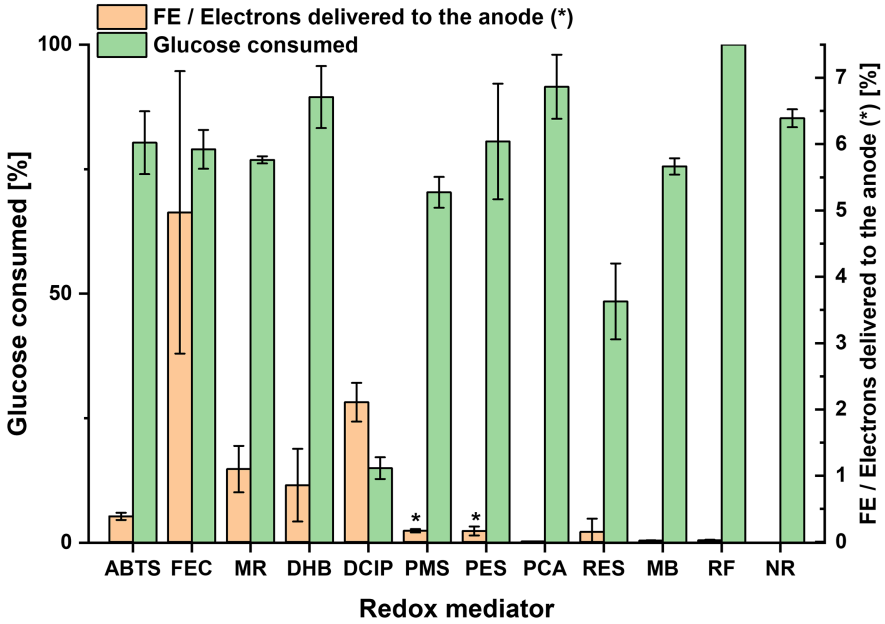

FIGURE 2 | The faradaic efficiency (FE) was the highest with potassium ferricyanide (1 mM). With the other tested mediators, it remained under 3%, on average. Negligible effects on glucose consumption as a result of cultivation with the redox mediator were observed except for RES and DCIP, with which less than 60% of initial glucose was consumed. The FE was calculated according to the equation described in the methods section, accounting for fermentation products. For PMS and PES, the total amount of electrons calculated for the fermentation products surpassed 100%. Therefore, for PMS and PES, the percentage of electrons delivered from consumed glucose to the anode is reported, without subtracting the organic acids from the available electron pool and are therefore marked with an asterisk (*). The values without taking into account the electrons delivered to organic acids are shown in Figure S5, which show the same overall trend. 2,2′-azino-bis(3-ethylbenzothiazoline-6-sulfonic acid) (ABTS), potassium ferricyanide (FEC), methylene blue (MB), neutral red (NR), resorufin (RES), phenazine carboxylic acid (PCA) and riboflavin (RF) ($n = 3$); methyl red (MR), 2,6-dichlorophenolindophenol (DCIP), phenazine ethosulfate (PES) and phenazine methosulfate (PMS) ($n = 4$); 2,3-dihydroxybenzoic acid (DHB) ($n = 5$). The error bars indicate the standard deviation of biological replicates.

biocompatibility may face mass-transfer limitations to the anode in scaled systems, potentially rendering them technically unviable regardless of optimization. While EC_{50}-determined concentrations would provide more rigorous control over cytotoxicity, the effort of establishing dose–response curves for the redox mediators would be more effectively applied after initial screening identifies promising candidates. Accordingly, EC_{50}-informed concentration selection remains an important next step for the most promising mediators to balance cell activity and current density output.

2.4 | Analysis of Chronoamperometry Results for FEC and PMS

The results extracted in the cycles per molecule and FE metrics are based on the integral of the current-time curves of all tested mediators, resulting in an evaluation of the overall system performance. However, to better understand how the mediated systems behave, two examples of the data obtained with the miniaturized system of redox mediators with distinct electrochemical and biological profiles were selected. Out of the screened mediators, FEC and PMS exhibited distinct electrochemical and biological profiles (Figure 3A–D). Controls lacking *V. natriegens* produced negligible currents; however, a linear increase in current was observed with FEC, attributable to the direct recycling of the mediator between electrodes [12]. Despite this abiotic contribution, the absorbance at characteristic wavelengths of the oxidized mediators did not change significantly over time, confirming the stability of the used mediators.

After inoculation, the generated current was inversely proportional to the measured absorbance at the mediator's characteristic wavelengths. This inverse relationship demonstrates that the current originates from mediator-based electron transfer, where the bacterial reduction of the oxidized mediator drives the electrochemical signal. Comparison with cell-free controls confirmed that the currents produced in biological experiments resulted from bacterial cells reducing the mediator rather than mere recirculation within the system. Notably, current generation was not limited to exogenous mediators as control experiments conducted without any added compounds still yielded measurable currents following inoculation (Figure 3B). This confirms that *V. natriegens* was capable of producing current via native EET mechanisms under these specific cultivation conditions.

Using FEC, current densities up to $104 \pm 20\,\mu A\,cm^{-2}$ were generated in this system with an optical density of 0.2 at 600 nm, which are in the range of current densities previously reached using FEC as redox mediator with *V. natriegens* in a stirred tank bioreactor setup (~$200\,\mu A\,cm^{-2}$) while following a very similar trend over time [7]. Conversely, PMS experiments exhibited a decline in current after approximately 2 h, coinciding with the accumulation of reduced PMS and the stagnation of cell growth, although glucose was still present in the medium (Figure 2). This

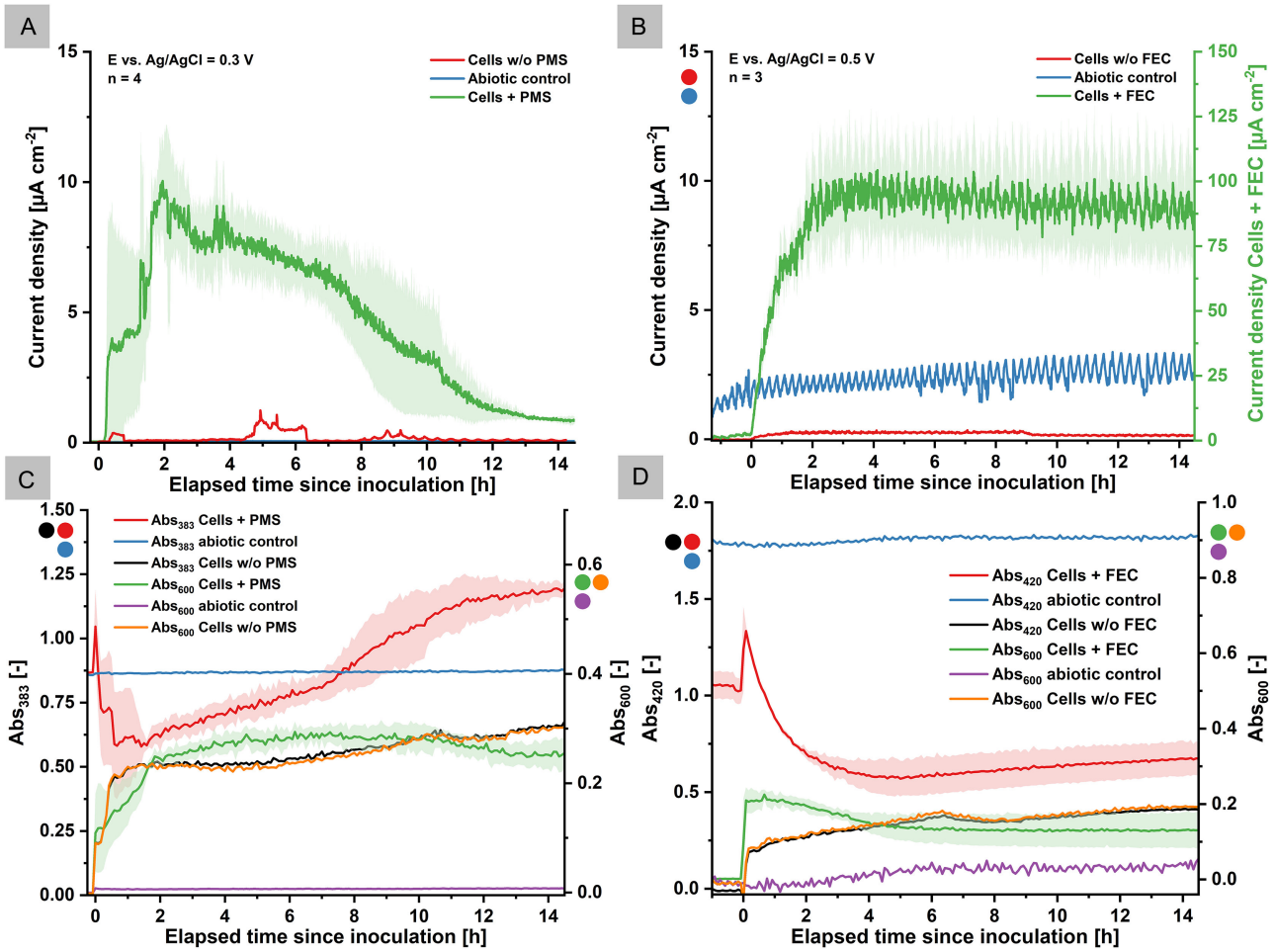

FIGURE 3 | The observed current originates from mediated electron transfer with PMS (A,C) and FEC (B,D). The subplots show the current density and online spectrophotometric monitoring of *Vibrio natriegens* cultivation in the miniaturized BES containing soluble redox mediators. Colored circles indicate the corresponding *Y*-axis for the plotted data. Cells were inoculated from minimal media precultures in the mid-exponential growth phase. Lines represent the mean of biological replicates ($n = 4$ for PMS; $n = 3$ for FEC), with shaded areas indicating the standard deviation. (A) Current density for cultures supplemented with 50 µM PMS and corresponding control experiments. (B) Current density profiles for cultures supplemented with 1000 µM FEC and corresponding control experiments. (C,D) Spectrophotometric data showing absorbance at 600 nm (Abs_{600}) for cell growth monitoring and at the characteristic wavelength specific to each mediator in the oxidized state ($Abs_{383/420}$).

downturn could be attributed to phenazine-induced cytotoxicity, a phenomenon well documented to impair cellular activity and viability [21]. While phenazines can generate reactive oxygen species (ROS) such as superoxide and hydrogen peroxide through the reduction of molecular oxygen, a process that should be minimized by continuous nitrogen sparging, trace oxygen diffusion into the system could still facilitate ROS-mediated auto-poisoning [20, 21]. Additionally, phenazine toxicity is not strictly dependent on oxygen. Meirelles and Newman demonstrated that phenazines like pyocyanin can cause cell death under strictly anoxic conditions if cells lack sufficient ATP or carbon catabolism capacity to power defense mechanisms [21]. This aligns well with the observed current time curve, increasing at the beginning when sufficient carbon source is present and then decreasing as the carbon source is progressively consumed and less energy can be channeled to defense mechanisms against phenazine cytotoxicity. Notably, a similar trend in the cultivation of *C. necator* with PMS in the same miniaturized setup used was observed, declining also after 2 h of cultivation and not maintaining stable current densities [12].

2.5 | In Silico Protein Folding

In order to determine if, despite the low sequence identity, the *V. natriegens* MtrCAB complex is structured comparable to the well-characterized one from *Shewanella* species (*Shewanella oneidensis*/*Shewanella baltica*) [22], the *V. natriegens* MtrCAB complex structure was predicted using Alphafold 3 (Figure 4). The predictions (Local Distance Difference Test (pLDDT) = 70–90, Interface Predicted Template Modeling (ipTM) = 0.79, Predicted Template Modeling (pTM) = 0.8) revealed that the heme groups of the *V. natriegens* MtrCAB complex direct electrons in a linear fashion from the periplasmic side to the extracellular space via the mtrA subunit, followed by spreading the electrons to multiple exit sites in MtrC.

Interestingly, the MtrC subunit is significantly rotated in respect of the MtrAB complex when compared to the *S. baltica* crystal structure (Figure S3). However, the full complex still renders the interaction with dissolved redox molecules feasible, regardless of their hydrophobicity or ability to traverse the outer membrane.

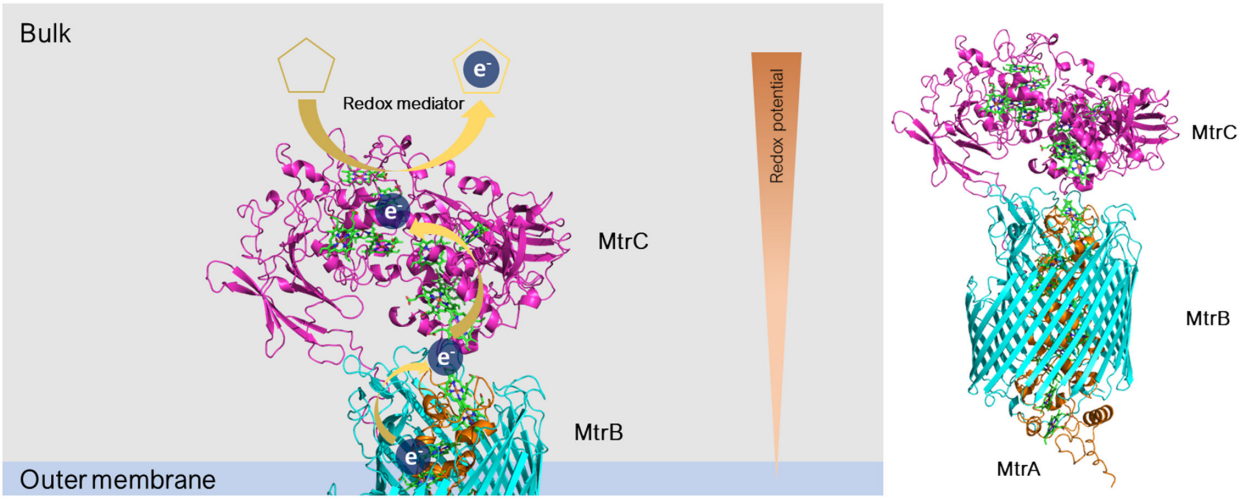

FIGURE 4 | Schematic overview of the predicted structure and its localization associated with the outer membrane in *V. natriegens*. Structure prediction was generated using AlphaFold 3. MtrC reaches into the bulk, presenting heme groups that can interact with dissolved redox mediators outside the cell envelope. The electrons are exported outside the cell from lower to higher redox potentials, where they can be delivered to suitable electron acceptors.

This extracellular accessibility aligns with experimental observations showing that mediators with a redox potential above −220 mV versus Ag/AgCl (3 M KCl) were reduced significantly more efficiently by *V. natriegens*. However, for all redox mediators other than ABTS that showed interaction with *V. natriegens* cells, the measured current likely arises from a combination of extracellular MtrCAB oxidation and electron uptake at periplasmic/intracellular sites. For instance, FEC interacts with various nonelectroactive organisms. Both gram-negative and gram-positive organisms, such as *P. putida*, *B. subtilis*, *and C. necator*, have demonstrated the ability to reduce FEC despite lacking extracellular cytochromes [12, 17, 23–26]. The critical role of membrane transport is highlighted by findings in *P. putida*, where porin overexpression increased current densities using FEC [17]. Although in the case of *V. natriegens*, the presence of an extracellular interaction partner eliminates the strict necessity for transport, transmembrane passage of the different redox shuttles likely still occurs either through porins or membrane diffusion for lipophilic molecules. This suggests that the total current output is a cumulative result of electron transfer taking place both outside the cell via MtrCAB and within the boundaries of the outer cell membrane.

3 | Conclusion

We have systematically evaluated twelve redox mediators to establish MET in *V. natriegens*. Among the candidates tested, potassium ferricyanide demonstrated superior performance, yielding the highest current densities and faradaic efficiencies. Significant electrochemical activity was also observed for methyl red, ABTS, and various phenazine compounds. Furthermore, we identified a specific redox potential window above −220 mV versus Ag/AgCl (3 M KCl), within which *V. natriegens* effectively reduces mediators.

The observed reduction of ABTS by *V. natriegens*, contrasted with the lack of activity in *C. necator* (which lacks dedicated EET machinery), suggests that ABTS could serve as a useful probe for EET capabilities in gram-negative bacteria. This aligns with computational folding studies, which support the hypothesis that *V. natriegens* utilizes the surface-exposed hemes from MtrCAB to interact directly with dissolved mediators in the bulk solution. While this screening provides a catalog of compatible redox shuttles, future research should focus on elucidating the extent to which these mediators interact with the MtrCAB complex versus periplasmic/intracellular interaction sites. Ultimately, these findings contribute to the development of high-efficiency bioelectrochemical processes by leveraging the robust interaction between the extremely fast-growing *V. natriegens* and potassium ferricyanide to optimize electron flux and system stability.

4 | Experimental Section

4.1 | Chemicals

Chemicals were purchased from Carl Roth GmbH & Co. KG (Germany), Sigma–Aldrich (USA), Chempur (Germany), Riedel-de Haën (Germany), Merck (Germany), and Alfa Aesar (USA).

4.2 | Preculture Preparation

A freeze-dried vial of *V. natriegens* DSM 759 was obtained from the Leibniz Institute DSMZ German Collection of Microorganisms and Cell Cultures. Cryo-cultures derived from this vial were kept at −80 °C before use. Under monoseptic conditions, a small aliquot of the cryo-stock was transferred into 500 µL of PBS buffer and resuspended. From this suspension, 100 µL was plated onto LB-agar (with additional 15 g/L NaCl), spread evenly using a sterile Drigalski spatula, and incubated overnight at 30 °C. For the liquid preculture, a single colony from the agar plate was transferred into 15 mL of modified M1 medium in a 100 mL shaking flask [5, 9] containing

10 g/L glucose, 13.21 g/L Na_2HPO_4, 6.59 g/L K_2HPO_4, 25.71 g/L NaCl, 1.18 g/L NH_4Cl, 1.63 g/L $MgSO_4$ 7·H_2O, 73.5 mg/L $CaCl_2$·H_2O, 50 mg/L EDTA, 8.3 mg/L $FeCl_3$, 0.84 mg/L $ZnCl_2$, 0.13 mg L $CuCl_2$, 0.1 mg/L, $CoCl_2$·6 H_2O, 0.1 mg/L H_3BO_3, and 0.016 mg/L $MnCl_2$·2 H_2O. The flask was incubated aerobically at 37 °C and 180 rpm. Cultivation proceeded until the optical density at 600 nm (OD_{600}) reached 2–3, typically requiring 6–8 h.

4.3 | eCuvette Setup and Cultivation Conditions

Screening experiments were conducted in a miniaturized system designed for the simultaneous online monitoring of absorbance and electrical current [11]. The setup was adapted to a Cary 60 spectrophotometer (Agilent Technologies, Santa Clara, USA) equipped with eight 4 mL polystyrene cuvettes. The cuvettes were sterilized overnight under UV light in a sterile bench. Each cuvette was fitted with screen-printed gold electrodes (C220 AT, Deutsche Metrohm GmbH & Co. KG, Germany) and an Ag/AgCl (3 M KCl) reference electrode. For riboflavin, confirmation experiments were additionally conducted using carbon screen-printed electrodes fitted into the same system (C110, German Metrohm GmbH & Co. KG, Germany). To maintain anaerobic conditions and ensure mixing within the channels, the system was continuously sparged with nitrogen at a flow rate of 5 mL min^{-1}. Before inoculation, the cuvettes were filled with M1 medium without NH_4Cl, temperature control was turned on at 30 °C, and sparged for at least 30 min with 99.999% N_2. The ammonium-free medium employed to control optical density measurements restricted *V. natriegens* to a nongrowing but metabolically active state. The cuvettes were incubated overnight at 30 °C, with photometric data acquisition performed every 5 min. The working concentrations for each redox mediator were adopted from [12], where they were determined based on maximal aqueous solubility and photometric assay detection limits. These standardized concentrations were retained across both organisms to enable comparison under matched screening conditions.

4.4 | Electrochemical and Photometric Analysis Methods

Electrochemical measurements were controlled using a multichannel potentiostat with eight channels (PalmSens BV, Netherlands) connected to a computer with the MultiTrace 4.5 Software (PalmSens BV, Netherlands). Chronoamperometry was employed to monitor current generation over time, with the working electrode potential set to a fixed value for mediator oxidation. The average cycle per molecule was calculated based on a previously established method [11]. The maximal reduction rate was calculated from the decline in the characteristic wavelengths for each mediator using calibration curves to calculate concentration decrease from absorbance changes. In the presence of cells, light scattering and intrinsic absorbance from biomass and medium components contribute an additional, largely wavelength-independent offset to the total absorbance signal rather than altering its slope. Biomass density changes on the timescale of the culture's doubling time (hours), which is orders of magnitude slower than the mediator reduction kinetics measured here. We therefore assume that the reduction rate, calculated from the slope of the absorbance decline, is not significantly affected by biomass accumulation over this timescale. This was confirmed experimentally by monitoring absorbance at the characteristic wavelengths in cell suspensions without mediator (e.g., Figure 3C,D), which showed a linear relationship with Abs_{600} (biomass). Additionally, cyclic voltammetry (CV) was performed to verify the presence of the redox couple and confirm the integrity of the electrical setup. CV scans were recorded at both the beginning and the end of each cultivation run. Each CV measurement consisted of five consecutive cycles scanned at a rate of 10 mV s^{-1}.

4.5 | HPLC Analysis and Calculation of Faradaic Efficiency (FE)

To quantify substrate consumption, samples were collected at the end of each experiment and centrifuged. The supernatant was stored at −20 °C until HPLC analysis. Glucose, organic acid, and ethanol concentrations were determined using an Agilent 1100 series HPLC system (Agilent Technologies, Waldbronn, Germany). Separation was achieved using a Rezex ROA-organic Acid Ht (8%) Phenomenex column maintained at 50 °C, with 5 mM H_2SO_4 serving as the mobile phase at a flow rate of 0.5 mL min^{-1} andana RI detector. The data was recorded and analyzed using the Chemstation software (C.01.07 27, Agilent Technologies, Santa Clara, CA, USA).

To calculate the FE, the charge contained in the main fermentation products was subtracted from the charge contained in the initial glucose according to the equation below.

$$FE\,(\%) = 100^{*}\frac{\int_{t_0}^{t_{end}} I}{96,485.33\frac{C}{mol}\left(24^{*}n_{Glucose} - \left(4^{*}n_{Acetate} + 10^{*}n_{Pyruvate} + 2^{*}n_{Formate} + 12^{*}n_{Ethanol}\right)\right)}$$

4.6 | Computational Protein Folding Prediction

To assess the theoretical interaction between the cellular electron-transfer machinery and dissolved redox mediators, computational protein structure predictions were performed using AlphaFold 3 and the AlphaFold Server [27]. The MtrCAB homologs in *V. natriegens* (WP_020332994, WP_014231553, and WP_020332993 for MtrC, MtrA, and MtrB, respectively) were previously identified in a study of EET pathways [5]. The signal peptides of each protein were identified using SignalP 6.0 [28] and removed prior to subjecting them to AlphaFold predictions. As MtrC and MtrA are decaheme proteins, 20 heme C cofactors (HEC) in total were included in the prediction. The resulting structural models were examined to determine the spatial accessibility of heme groups within the folded protein complex in the bulk.

The AlphaFold Server provides confidence metrics to evaluate modeled structures. The modified Local Distance Difference Test (pLDDT) delivers information about the reliability of each residues position, while Predicted Template Modeling (pTM) describes the whole-structure accuracy and Interface Predicted Template Modeling (ipTM) the interaction accuracy between chains. Generally, the pLDDT metric is in a range between 0 and 100, and in general, a value over 70 indicates a good fit, while values above 90 are considered to have very high confidence [27]. For the pTM and ipTM metrics, values range from 0 to 1, and values above 0.5 are generally considered reliable, as this threshold typically indicates that the predicted structures share the same fold or represent a correct interface rather than a random structural match. Further information about these metrics can be found in the original AlphaFold3 and TM-score literature [27, 29, 30]. The AlphaFold 3 data generated in this study can be found on Zenodo under the DOI: https://doi.org/10.5281/zenodo.20526205.

Acknowledgments

The authors thank the German Research Foundation (DFG) for funding this work as part of the project "eBiotech SPP 240"—Project number 536355345. Open Access funding provided by the DEAL Project. Large language models (Qwen3.5 397B A17B, locally hosted, accessed from 02.05.2026 to 01.07.2026 and Google's NotebookLM 2.0 (accessed from 08.05.2026 to 01.07.2026)) were used to assist with language editing, structuring, and summarizing general content in this manuscript. These tools were not used to create the original draft or develop original scientific interpretations. All content was critically reviewed, verified, and approved by the authors, who take full responsibility for the integrity and accuracy of the work.

Open Access funding enabled and organized by Projekt DEAL.

Funding

This study was supported by Deutsche Forschungsgemeinschaft (536355345).

Conflicts of Interest

The authors declare no conflicts of interest.

Data Availability Statement

The data presented in this study will be made available upon reasonable request to the authors.

References

1. A. Faber, R. J. Politan, D. Stukenberg, et al., "Expanding Genetic Engineering Capabilities in *Vibrio Natriegens* With the Vnat Collection," *Nucleic Acids Research* 53 (2025): gkaf580, https://doi.org/10.1093/nar/gkaf580.

2. F. Thoma and B. Blombach, "Metabolic Engineering of *Vibrio Natriegens*," *Essays in Biochemistry* 65 (2021): 381–392, https://doi.org/10.1042/EBC20200135.

3. R. G. Eagon, "*Pseudomonas Natriegens*, a Marine Bacterium With a Generation Time of less Than 10 Min," *Journal of Bacteriology* 83 (1962): 736–737, https://doi.org/10.1128/jb.83.4.736-737.1962.

4. C. P. Long, J. E. Gonzalez, R. M. Cipolla, and M. R. Antoniewicz, "Metabolism of the Fast-Growing Bacterium *Vibrio Natriegens* Elucidated by 13C Metabolic Flux Analysis," *Metabolic Engineering* 44 (2017): 191–197, https://doi.org/10.1016/j.ymben.2017.10.008.

5. B. E. Conley, M. T. Weinstock, D. R. Bond, J. A. Gralnick, and R. M. Kelly, "A Hybrid Extracellular Electron Transfer Pathway Enhances the Survival of *Vibrio Natriegens*," *Applied and Environmental Microbiology* 86 (2020): e01253, https://doi.org/10.1128/AEM.01253-20.

6. I. Vassilev, N. J. H. Averesch, P. Ledezma, and M. Kokko, "Anodic Electro-Fermentation: Empowering Anaerobic Production Processes via Anodic Respiration," *Biotechnology Advances* 48 (2021): 107728, https://doi.org/10.1016/j.biotechadv.2021.107728.

7. A. Gemünde, J. Gail, and D. Holtmann, "Anodic Respiration of *Vibrio Natriegens* in a Bioelectrochemical System," *ChemSusChem* 16 (2023): e202300181, https://doi.org/10.1002/cssc.202300181.

8. A. Gemünde, B. Lai, L. Pause, J. Krömer, and D. Holtmann, "Redox Mediators in Microbial Electrochemical Systems," *ChemElectroChem* 9 (2022): e202200216, https://doi.org/10.1002/celc.202200216.

9. L. Zhang, Y. Zhang, Y. Liu, et al., "High Power Density Redox-Mediated *Shewanella* Microbial Flow Fuel Cells," *Nature Communications* 15 (2024): 8302, https://doi.org/10.1038/s41467-024-52498-w.

10. Z. Gong, R. Xie, Y. Zhang, M. Wang, and T. Tan, "Identification of Emerging Industrial Biotechnology Chassis *Vibrio Natriegens* as a Novel High Salt-Tolerant and Feedstock Flexibility Electroactive Microorganism for Microbial Fuel Cell," *Microorganisms* 11 (2023): 490, https://doi.org/10.3390/microorganisms11020490.

11. A. Gemünde, J. Gail, J. Janek, and D. Holtmann, "e-Cuvettes Parallelize Electrochemical and Photometric Measurements in Cuvettes and Facilitate Applications in Bio-Electrochemistry," *Biosensors and Bioelectronics: X* 14 (2023): 100378, https://doi.org/10.1016/j.biosx.2023.100378.

12. A. Gemünde, J. Gail, and D. Holtmann, "Redox Mediator Interaction With *Cupriavidus Necator* – Spectroelectrochemical Online Analysis," *Electrochemistry Communications* 162 (2024): 107705, https://doi.org/10.1016/j.elecom.2024.107705.

13. S. D. Roller, H. P. Bennetto, G. M. Delaney, J. R. Mason, J. L. Stirling, and C. F. Thurston, "Electron-Transfer Coupling in Microbial Fuel Cells: 1. Comparison of Redox-Mediator Reduction Rates and Respiratory Rates of Bacteria," *Journal of Chemical Technology and Biotechnology* 34 (1984): 3–12, https://doi.org/10.1002/jctb.280340103.

14. E. Marsili, D. B. Baron, I. D. Shikhare, D. Coursolle, J. A. Gralnick, and D. R. Bond, "*Shewanella* Secretes Flavins that Mediate Extracellular Electron Transfer," *Proceedings of the National Academy of Sciences* 105 (2008): 3968–3973, https://doi.org/10.1073/pnas.0710525105.

15. I. Casas-Rodrigo, T. Vornholt, K. Castiglione, et al., "Permeabilisation of the Outer Membrane of *Escherichia Coli* for Enhanced Transport of Complex Molecules," *Microbial Biotechnology* 18 (2025): e70122, https://doi.org/10.1111/1751-7915.70122.

16. A. Gemünde, E. Rossini, O. Lenz, S. Frielingsdorf, and D. Holtmann, "Chemoorganotrophic Electrofermentation by *Cupriavidus Necator* Using Redox Mediators," *Bioelectrochemistry* 158 (2024): 108694, https://doi.org/10.1016/j.bioelechem.2024.108694.

17. A. Weimer, J. Krömer, B. Lai, and C. Wittmann, "The TonB -Dependent Transport System Facilitates the Uptake of Inorganic Metal Mediators in, *Pseudomonas Putida*, KT2440 in a Bioelectrochemical System," *Microbial Biotechnology* 18 (2025): e70206, https://doi.org/10.1111/1751-7915.70206.

18. R. S. Hartshorne, C. L. Reardon, D. Ross, et al., "Characterization of an Electron Conduit Between Bacteria and the Extracellular Environment," *Proceedings of the National Academy of Sciences* 106 (2009): 22169–22174, https://doi.org/10.1073/pnas.0900086106.

19. B. Reuillard, K. H. Ly, P. Hildebrandt, L. J. C. Jeuken, J. N. Butt, and E. Reisner, "High Performance Reduction of H_2O_2 With an Electron

Transport Decaheme Cytochrome on a Porous ITO Electrode," *Journal of the American Chemical Society* 139 (2017): 3324–3327, https://doi.org/10.1021/jacs.6b12437.

20. Y. Wang and D. K. Newman, "Redox Reactions of Phenazine Antibiotics With Ferric (Hydr)oxides and Molecular Oxygen," *Environmental Science & Technology* 42 (2008): 2380–2386, https://doi.org/10.1021/es702290a.

21. L. A. Meirelles and D. K. Newman, "Both Toxic and Beneficial Effects of Pyocyanin Contribute to the Lifecycle of *Pseudomonas Aeruginosa*," *Molecular Microbiology* 110 (2018): 995–1010, https://doi.org/10.1111/mmi.14132.

22. M. J. Edwards, G. F. White, J. N. Butt, D. J. Richardson, and T. A. Clarke, "The Crystal Structure of a Biological Insulated Transmembrane Molecular Wire," *Cell* 181 (2020): 665–673.e10, https://doi.org/10.1016/j.cell.2020.03.032.

23. L. Gu, X. Xiao, S. Yup Lee, B. Lai, and C. Solem, "Superior Anodic Electro-Fermentation by Enhancing Capacity for Extracellular Electron Transfer," *Bioresource Technology* 389 (2023): 129813, https://doi.org/10.1016/j.biortech.2023.129813.

24. B. Lai, A. V. Nguyen, and J. O. Krömer, "Characterizing the Anoxic Phenotype of *Pseudomonas Putida* Using a Bioelectrochemical System," *Methods and Protocols* 2 (2019): 26, https://doi.org/10.3390/mps2020026.

25. Y. Sun, C. Liu, I. Vassilev, A. J. Rissanen, J. Luo, and M. Kokko, "Enhanced Extracellular Respiration of Engineered *Bacillus Subtilis* via Anodic Electro-Fermentation With pH Optimisation," *Biotechnology for Biofuels and Bioproducts* 19 (2026): 8, https://doi.org/10.1186/s13068-025-02731-5.

26. I. Vassilev, G. Gießelmann, S. K. Schwechheimer, C. Wittmann, B. Virdis, and J. O. Krömer, "Anodic Electro-Fermentation: Anaerobic Production of L-Lysine by Recombinant *Corynebacterium Glutamicum*," *Biotechnology and Bioengineering* 115 (2018): 1499–1508, https://doi.org/10.1002/bit.26562.

27. J. Abramson, J. Adler, J. Dunger, et al., "Accurate Structure Prediction of Biomolecular Interactions With AlphaFold 3," *Nature* 630 (2024): 493–500, https://doi.org/10.1038/s41586-024-07487-w.

28. F. Teufel, J. J. lmagro Armenteros, A. R. Johansen, et al., "SignalP 6.0 predicts All Five Types of Signal Peptides Using Protein Language Models," *Nature Biotechnology* 40 (2022): 1023–1025, https://doi.org/10.1038/s41587-021-01156-3.

29. Y. Zhang and J. Skolnick, "Scoring Function for Automated Assessment of Protein Structure Template Quality," *Proteins* 57 (2004): 702–710, https://doi.org/10.1002/prot.20264.

30. J. Xu and Y. Zhang, "How Significant Is a Protein Structure Similarity With TM-Score = 0.5?," *Bioinformatics* 26 (2010): 889–895, https://doi.org/10.1093/bioinformatics/btq066.

Supporting Information

Additional supporting information can be found online in the Supporting Information section.